Reduced-Order Models for Nonlinear Flutter of Composite Laminates with Curvilinear Fibers

Hamed Akhavan* and Pedro Ribeiro†
Universidad do Porto, 4200-465 Porto, Portugal

DOI: 10.2514/1.J057755

Approximation errors due to using reduced-order, instead of full-order, models in the nonlinear flutter problem of variable-stiffness composite laminates (VSCLs) are qualitatively and quantitatively discussed. These VSCLs are made of composite laminates with curvilinear fibers. A third-order shear deformation theory (TSDT) and a *p*-version finite element are used to model the laminate and discretize its displacements and rotations. The VSCLs are subjected to a supersonic airflow and the aerodynamic pressure is approximated using the linear piston theory. The equations of motion of the self-excited vibrational system are formed using the principle of virtual work. In this study, static condensation and/or a modal summation method are used to reduce the number of degrees of freedom of the full-order model. The equations of motion are solved using a method to calculate the amplitudes of limit-cycle oscillations (LCOs), and to study the dynamic responses, stresses, and damage indexes based on a failure criterion. Approximations are calculated for LCO amplitudes of VSCL plates with various boundary conditions, laminate thickness, and initial deflection (geometric imperfection). Viscous damping can have a major importance in this problem, and the approximation errors are discussed when viscous damping is included or excluded from the equations of motion.

Nomenclature

a, b	=	length and width of the plate, respectively, m
c	=	$4/3h^2$
D	=	plate stiffness; $E_1 h^3/12(1-\nu^2)$
E_1, E_2	=	major and minor Young's moduli, respectively, in material coordinates 1 and 2, GPa
G_{12}, G_{13}, G_{23}	=	shear moduli, in material coordinates 1, 2, and 3, GPa
h	=	thickness of the plate, m
h_i	=	magnitude of the imperfection half-wave, m
M	=	Mach number
$\boldsymbol{N}^i(x, y)$	=	vector of shape functions (in which $\boldsymbol{i}$ is equal to $\boldsymbol{u}$, $\boldsymbol{v}$, $\boldsymbol{w}$, $\boldsymbol{\phi}_x$, and $\boldsymbol{\phi}_y$)
p	=	aerodynamic pressure, Pa
q	=	dynamic pressure; $\rho_\infty U_\infty^2/2$
$\boldsymbol{q}_i(t)$	=	generalized displacement vectors (in which $\boldsymbol{i}$ is equal to $\boldsymbol{u}$, $\boldsymbol{v}$, $\boldsymbol{w}$, $\boldsymbol{\phi}_x$, and $\boldsymbol{\phi}_y$)
S	=	shear strength, MPa
T_0, T_1	=	characteristic angles of the fiber path, deg
t	=	time, s
U_∞	=	freestream velocity, m/s
u, v, w	=	displacement components in the x, y, z directions
u^0, v^0, w^0	=	displacement values at the midplane
W	=	limit-cycle-oscillation amplitude, m
w_i	=	initial deflection
X_t, X_c	=	longitudinal tensile and compressive strengths, MPa
x, y, z	=	Cartesian coordinate system
Y_t, Y_c	=	transverse tensile and compressive strengths, MPa
β	=	$\sqrt{M^2-1}$
$\theta(x)$	=	angle of the reference fiber path
λ	=	nondimensional dynamic pressure; $2qa^3/\beta D$
μ	=	$a\rho_\infty/h\rho$
ν	=	Poisson's ratio
ρ	=	density of the plate, kg/m^3
ρ_∞	=	ambient density of air, kg/m^3
ϕ_x, ϕ_y	=	independent rotations of the normal to the middle surface about the y and x axes
Ω	=	surface of a plate
ω	=	angular velocity, rad/s
ω_n	=	nondimensional linear natural frequency; $\omega h\sqrt{\rho/G}$

Superscript

T	=	transpose of matrix or vector

I. Introduction

THIS paper evaluates the accuracy and efficiency of reduced-order models (ROMs) for nonlinear flutter of variable-stiffness composite laminates (VSCLs) subjected to a supersonic airflow. A linear (small-amplitude) structure model associated with a linear aerodynamic model indicates a critical aerodynamic pressure value (linear flutter pressure) above which the plate oscillation becomes unstable and its amplitude grows exponentially with time. The inclusion of geometric nonlinearities makes the oscillation amplitude restrained and bounded into a limit-cycle oscillation (LCO) [1]. The mentioned geometric nonlinearity comes from the nonlinear coupling between out-of-plane bending and in-plane stretching of the plate. A full-order finite element (FE) model, which includes all the physical degrees of freedom (DOFs), can successfully predict the rich nonlinear dynamics of a fluttering plate. To solve such a usually large full-order model (FOM), high computational efforts and expenses are normally needed. ROMs—coming from FOMs weakened with order reduction techniques—as well as a small FOM (i.e., an FOM with a few DOFs) can loosely predict such a nonlinear and enriched behavior. The paper aimed at investigating, quantitatively and qualitatively, the approximation errors due to using ROMs instead of their associated FOM in the nonlinear flutter problem of VSCLs.

VSCLs with curvilinear fibers, which can be made, for example, by an automated fiber placement [2] machine, are among the composites that have been recently used in aerospace industry. This concept of composites permits redistribution of stresses from high-stress locations in a panel to other stiffer areas (e.g., from the corners to the edges of a panel). In another example, fiber paths around a hole

Received 23 July 2018; revision received 29 January 2019; accepted for publication 10 February 2019; published online 28 March 2019.

*Postdoctoral Researcher, INEGI/DEMec, Faculdade de Engenharia, Rua Dr. Roberto Frias; hamed@fe.up.pt.

†Associate Professor, DEMec/INEGI, Faculdade de Engenharia, Rua Dr. Roberto Frias; pmleal@fe.up.pt.

in a plate or around windows in an airplane fuselage can be curved to avoid stress concentration [3]. Supersonic airflow allows one to use a simple aerodynamic model and occurs, for example, in modern fighter aircraft or space shuttles, in the latter at least during portions of their reentry. This study targets VSCLs, but its conclusions can be extended to panels in other materials.

In this paper, the order of FOMs is reduced by static condensation, or by transfer to modal coordinates, or by both procedures. For simplification, the following designations are assigned to the models: 1) FOM, 2) statically condensed ROM (ROM1), 3) ROM in modal coordinates (ROM2), and 4) statically condensed ROM in modal coordinates (ROM3).

It is obvious that, to have an exact-enough solution to flutter of a nonlinear system, enough DOFs are necessary in the FOM. Using less DOFs in the FOM or ROMs helps the researchers to find an approximated solution of the nonlinear systems using computers with less memory or less CPU speed. Although LCO amplitude approximations by reduced-order nonlinear systems have been already mentioned (e.g., in [4–7]), they have not yet been quantitatively analyzed. Besides the LCO amplitudes, the degrees of approximation on stresses and damage indexes have not yet been qualitatively and quantitatively expressed.

ROMs for nonlinear systems of airfoils or wing models are exploited in Refs. [8–16] for prediction of flutter, LCOs, and transient responses. The nonlinear flutter of panels is analyzed using FOMs and ROMs in Refs. [17–51]. Generally, six to eight modes have been used in Refs. [17–51]. Structural modal coordinates are usually used in these references; exceptions are Refs. [20,25,32,48–51], in which either aeroelastic modes or proper orthogonal decomposition (POD) was employed instead of structural modes. In these references, mostly classical plate/laminate theory (CPT/CLT) or first-order shear deformation theory (FSDT) is used. In the current paper, the authors use a third-order shear deformation theory (TSDT) to assess the effect of geometry (thickness-to-length ratio) on the approximations given by ROMs; a TSDT has the advantages of leading to more accurate stress computation and of being applicable to thicker plates. Reference [30] gives a review on the nonlinear flutter analysis of plates using reduced-order systems by modal coordinates, in which the authors draw attention to the importance of initial imperfections, structural/viscous damping, and support conditions on such analysis. Regarding boundary conditions, simply supported, clamped, and cantilevered conditions were considered in [17–51]. Wherever cantilevered conditions were applied, the researchers were forced to use more DOFs. In these references, structural/viscous damping was generally neglected.

The main goal of this study was to quantify and qualify the degree of approximation of ROMs with respect to their associated FOMs in VSCL plates. For this purpose, an in-house Fortran code that was developed and validated in the past by the authors is now updated to obtain the nonlinear flutter response of imperfect VSCLs. In the current paper, Newmark method is used for the solution of the developed models. The mentioned code has been validated and used for the analyses of linear vibration [52], static deflection [53], stresses and failure [54], free and forced nonlinear vibration with or without initial imperfection [55–60], and, finally, for the analysis of linear flutter [61]. In recent years, some works [40,62–64] have been published on linear flutter of VSCLs, but up to now and up to the best of the authors' knowledge, no work exists, in the literature, on the nonlinear flutter of VSCLs. Hence, the authors believe that this study is necessary to help researchers who want to use ROMs in VSCLs as well as in traditional plates.

Section II of this paper is dedicated to FOM and ROM formulation of VSCLs, subjected to a supersonic airflow. Section III is devoted to validation of the present linear and nonlinear FOMs, by comparison with data available in the literature. In Sec. IV, results are presented and discussed for FOM and ROMs of a VSCL plate, with subsections devoted to: 1) effect of different boundary conditions, 2) effect of inclusion of viscous damping, 3) effect of geometrical imperfection, 4) effect of plate thickness, 5) stress, and 6) failure. Final comments are written in the last section, with some useful observations on the number of modes (DOFs) and margins of validity of the ROMs.

II. Equations of Motion of VSCLs Subjected to a Supersonic Flow

A rectangular laminate, with a Cartesian coordinate system (x, y) with origin located in the geometric center of the undeformed plate, is shown in Fig. 1. The laminate is symmetric about its middle plane. The reference fiber path is curvilinear and its angle is defined, with respect to the x axis, as $\theta(x) = (T_1 - T_0)[(x + a/2)/a] + T_0$. This form of reference curvilinear fiber path is selected after Ref. [61], in which two types of reference fiber paths were analyzed and the current path demonstrated better linear flutter characteristics (fig. 3 of Ref. [61]). The orientation in the reference fiber path changes linearly from T_0 at the left edge to T_1 at the right edge of any ply in the laminate, where each ply has its own characteristic fiber angles $\langle T_0, T_1 \rangle$. To define the other fiber paths, the reference fiber path shifts in the y direction [65].

A displacement field, based on a TSDT [66,67], is used as follows:

$$\begin{aligned} u(x,y,z,t) &= u^0(x,y,t) + z\phi_x(x,y,t) \\ &\quad - cz^3\left(\phi_x(x,y,t) + \frac{\partial w^0(x,y,t)}{\partial x}\right) \\ v(x,y,z,t) &= v^0(x,y,t) + z\phi_y(x,y,t) \\ &\quad - cz^3\left(\phi_y(x,y,t) + \frac{\partial w^0(x,y,t)}{\partial y}\right) \\ w(x,y,z,t) &= w^0(x,y,t) + w_i(x,y) \end{aligned} \tag{1}$$

Midplane displacements and rotations are discretized using a p-version FE [68,69] as

$$\begin{Bmatrix} u^0(x,y,t) \\ v^0(x,y,t) \\ w^0(x,y,t) \\ \phi_x(x,y,t) \\ \phi_y(x,y,t) \end{Bmatrix} = \begin{bmatrix} \boldsymbol{N}^u(x,y)^T & \mathbf{0} & \mathbf{0} & \mathbf{0} & \mathbf{0} \\ \mathbf{0} & \boldsymbol{N}^u(x,y)^T & \mathbf{0} & \mathbf{0} & \mathbf{0} \\ \mathbf{0} & \mathbf{0} & \boldsymbol{N}^w(x,y)^T & \mathbf{0} & \mathbf{0} \\ \mathbf{0} & \mathbf{0} & \mathbf{0} & \boldsymbol{N}^{\phi_x}(x,y)^T & \mathbf{0} \\ \mathbf{0} & \mathbf{0} & \mathbf{0} & \mathbf{0} & \boldsymbol{N}^{\phi_y}(x,y)^T \end{bmatrix} \begin{Bmatrix} \boldsymbol{q}_u(t) \\ \boldsymbol{q}_v(t) \\ \boldsymbol{q}_w(t) \\ \boldsymbol{q}_{\phi_x}(t) \\ \boldsymbol{q}_{\phi_y}(t) \end{Bmatrix} \tag{2}$$

The stress–strain relation in an orthotropic lamina (in material coordinates, with axes 1, 2, and 3, in which 1 is the fiber direction, 2 is perpendicular to the fiber direction, and 3 is normal to the surface; Fig. 1) is valid in each arbitrary point of the ply made of curvilinear fibers [70]. Because of the rotation of the fiber path $\theta(x)$, stress and strain in material coordinates can be transformed to global coordinates (x and y in Fig. 1) using a transformation matrix [70]. A strain–displacement relation retaining von Kármán nonlinear terms is considered in this study.

Air is considered to flow on the front side of the plate, and constant pressure equal to the undisturbed air pressure is set at the other (back) side. The pressure difference between the front and back surfaces of the plate due to a supersonic flow (highly unsteady) with velocity U_∞, in x direction, can be defined using the linear piston theory [71–73] as

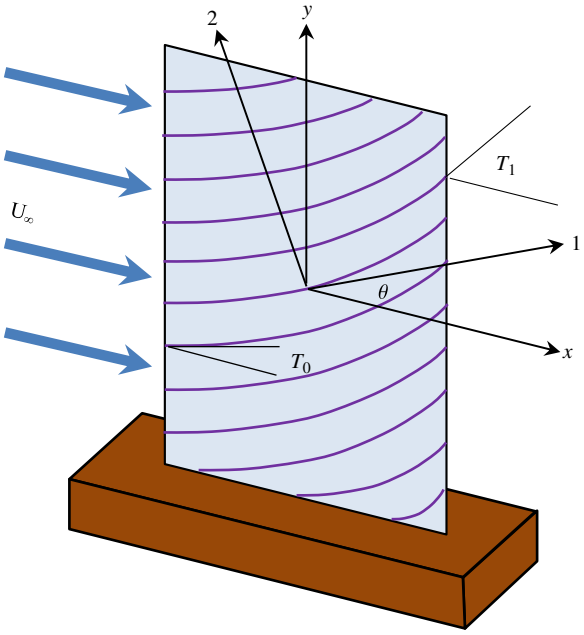

Fig. 1 Geometry of a cantilever VSCL plate and its fiber paths.

$$\Delta p(x,y,t) = -\frac{2q}{\beta}\left(\frac{M^2-2}{M^2-1}\frac{1}{U_\infty}\frac{\partial w(x,y,t)}{\partial t} + \frac{\partial w(x,y,t)}{\partial x}\right) \quad (3)$$

Defining the virtual works of inertia forces, internal forces and external aerodynamic forces, and using the principle of virtual work lead to the full-order equations of motion of self-excitation vibration in the form of

$$\begin{bmatrix} \boldsymbol{M}^{11} & \boldsymbol{0} & \boldsymbol{0} & \boldsymbol{0} & \boldsymbol{0} \\ & \boldsymbol{M}^{22} & \boldsymbol{0} & \boldsymbol{0} & \boldsymbol{0} \\ & & \boldsymbol{M}^{33} & \boldsymbol{M}^{34} & \boldsymbol{M}^{35} \\ & & & \boldsymbol{M}^{44} & \boldsymbol{0} \\ \text{sym} & & & & \boldsymbol{M}^{55} \end{bmatrix} \begin{Bmatrix} \ddot{\boldsymbol{q}}_u(t) \\ \ddot{\boldsymbol{q}}_v(t) \\ \ddot{\boldsymbol{q}}_w(t) \\ \ddot{\boldsymbol{q}}_{\phi_x}(t) \\ \ddot{\boldsymbol{q}}_{\phi_y}(t) \end{Bmatrix} + \begin{bmatrix} \boldsymbol{0} & \boldsymbol{0} & \boldsymbol{0} & \boldsymbol{0} & \boldsymbol{0} \\ & \boldsymbol{0} & \boldsymbol{0} & \boldsymbol{0} & \boldsymbol{0} \\ & & \boldsymbol{F}^{33}_{\text{unsteady}} & \boldsymbol{0} & \boldsymbol{0} \\ & & & \boldsymbol{0} & \boldsymbol{0} \\ \text{sym} & & & & \boldsymbol{0} \end{bmatrix} \begin{Bmatrix} \dot{\boldsymbol{q}}_u(t) \\ \dot{\boldsymbol{q}}_v(t) \\ \dot{\boldsymbol{q}}_w(t) \\ \dot{\boldsymbol{q}}_{\phi_x}(t) \\ \dot{\boldsymbol{q}}_{\phi_y}(t) \end{Bmatrix}$$
$$+ \left(\begin{bmatrix} \boldsymbol{K}^{11}_L & \boldsymbol{K}^{12}_L & \boldsymbol{K}^{13}_L & \boldsymbol{0} & \boldsymbol{0} \\ & \boldsymbol{K}^{22}_L & \boldsymbol{K}^{23}_L & \boldsymbol{0} & \boldsymbol{0} \\ & & \boldsymbol{K}^{33}_L & \boldsymbol{K}^{34}_L & \boldsymbol{K}^{35}_L \\ & & & \boldsymbol{K}^{44}_L & \boldsymbol{K}^{45}_L \\ \text{sym} & & & & \boldsymbol{K}^{55}_L \end{bmatrix} + \begin{bmatrix} \boldsymbol{0} & \boldsymbol{0} & \boldsymbol{K}^{13}_{NL}(\boldsymbol{q}_w) & \boldsymbol{0} & \boldsymbol{0} \\ \boldsymbol{0} & \boldsymbol{0} & \boldsymbol{K}^{23}_{NL}(\boldsymbol{q}_w) & \boldsymbol{0} & \boldsymbol{0} \\ \boldsymbol{K}^{31}_{NL}(\boldsymbol{q}_w) & \boldsymbol{K}^{32}_{NL}(\boldsymbol{q}_w) & \boldsymbol{K}^{33}_{NL}(\boldsymbol{q}_w) & \boldsymbol{0} & \boldsymbol{0} \\ \boldsymbol{0} & \boldsymbol{0} & \boldsymbol{0} & \boldsymbol{0} & \boldsymbol{0} \\ \boldsymbol{0} & \boldsymbol{0} & \boldsymbol{0} & \boldsymbol{0} & \boldsymbol{0} \end{bmatrix} + \begin{bmatrix} \boldsymbol{0} & \boldsymbol{0} & \boldsymbol{0} & \boldsymbol{0} & \boldsymbol{0} \\ & \boldsymbol{0} & \boldsymbol{0} & \boldsymbol{0} & \boldsymbol{0} \\ & & \boldsymbol{F}^{33}_{\text{steady}} & \boldsymbol{0} & \boldsymbol{0} \\ & & & \boldsymbol{0} & \boldsymbol{0} \\ \text{sym} & & & & \boldsymbol{0} \end{bmatrix} \right)$$
$$\times \begin{Bmatrix} \boldsymbol{q}_u(t) \\ \boldsymbol{q}_v(t) \\ \boldsymbol{q}_w(t) \\ \boldsymbol{q}_{\phi_x}(t) \\ \boldsymbol{q}_{\phi_y}(t) \end{Bmatrix} = \boldsymbol{0} \quad (4)$$

Mass, linear, and nonlinear stiffness submatrices, $\boldsymbol{M}$, $\boldsymbol{K}_L$, and $\boldsymbol{K}_{NL}$, have already been established in terms of the p-version FE shape functions and can be found, for example, in Ref. [70]. The aerodynamic submatrices are defined as

$$\boldsymbol{F}^{33}_{\text{steady}} = \frac{2q}{\beta}\int \boldsymbol{N}^w \boldsymbol{N}^{wT}_{,x}\,\mathrm{d}\Omega$$
$$\boldsymbol{F}^{33}_{\text{unsteady}} = \frac{2q}{\beta}\frac{M^2-2}{M^2-1}\frac{1}{U_\infty}\int \boldsymbol{N}^w \boldsymbol{N}^{wT}\,\mathrm{d}\Omega \quad (5)$$

in which, x means $\partial/\partial x$. In a simplified form, the equations of motion of the self-exciting vibration can be written as

$$\boldsymbol{M}\ddot{\boldsymbol{q}}(t) + \boldsymbol{F}_{\text{unsteady}}\dot{\boldsymbol{q}}(t) + \left(\boldsymbol{K}_L + \boldsymbol{K}_{NL} + \boldsymbol{F}_{\text{steady}}\right)\boldsymbol{q}(t) = \boldsymbol{0} \quad (6)$$

A. Full-Order Model

In this particular study, seven one-dimensional shape functions in x and y coordinates [i.e., 49 two-dimensional shape functions or elements in $\boldsymbol{N}(x,y)$] are used for discretization of each of the five displacement and rotation variables in Eq. (2). This leads to an FOM coming from Eq. (6) with $5 \times 7^2 = 245$ DOFs (physical DOFs from p-version FE). Convergence of a model of VSCLs with this number of DOF was demonstrated by the authors in Ref. [70] in the absence of aeroelastic loads, and later in the presence of aerodynamic loads (but not shown due to restrictions in space).

B. Statically Condensed ROM

Static condensation [74] is generally used where in-plane accelerations are not very pronounced and the corresponding in-plane inertia can be neglected [75]. This technique reduces the number of equations (and consequently, the number of DOFs) and changes the bandwidth of the stiffness matrix. Putting the in-plane inertia equal to zero, one obtains in-plane displacements [from Eq. (4)] by

$$\begin{Bmatrix} \boldsymbol{q}_u(t) \\ \boldsymbol{q}_v(t) \end{Bmatrix} = -\begin{bmatrix} \boldsymbol{K}^{11}_L & \boldsymbol{K}^{12}_L \\ \boldsymbol{K}^{21}_L & \boldsymbol{K}^{22}_L \end{bmatrix}^{-1} \begin{Bmatrix} \boldsymbol{K}^{13}_L + \boldsymbol{K}^{13}_{NL}(\boldsymbol{q}_w) \\ \boldsymbol{K}^{23}_L + \boldsymbol{K}^{23}_{NL}(\boldsymbol{q}_w) \end{Bmatrix} \boldsymbol{q}_w(t) \quad (7)$$

The equations of motion that result from Eq. (4), in which the effect of in-plane displacements is taken into account, but not in-plane inertia, are

$$\begin{bmatrix} \boldsymbol{M}^{33} & \boldsymbol{M}^{34} & \boldsymbol{M}^{35} \\ & \boldsymbol{M}^{44} & \boldsymbol{0} \\ \text{sym} & & \boldsymbol{M}^{55} \end{bmatrix} \begin{Bmatrix} \ddot{\boldsymbol{q}}_w(t) \\ \ddot{\boldsymbol{q}}_{\phi_x}(t) \\ \ddot{\boldsymbol{q}}_{\phi_y}(t) \end{Bmatrix} + \begin{bmatrix} \boldsymbol{F}^{33}_{\text{unsteady}} & \boldsymbol{0} & \boldsymbol{0} \\ & \boldsymbol{0} & \boldsymbol{0} \\ \text{sym} & & \boldsymbol{0} \end{bmatrix} \begin{Bmatrix} \dot{\boldsymbol{q}}_w(t) \\ \dot{\boldsymbol{q}}_{\phi_x}(t) \\ \dot{\boldsymbol{q}}_{\phi_y}(t) \end{Bmatrix}$$
$$+ \begin{bmatrix} \boldsymbol{K}^{33}_{LS} + \boldsymbol{K}^{33}_{NLS}(\boldsymbol{q}_w) + \boldsymbol{F}^{33}_{\text{steady}} & \boldsymbol{K}^{34}_L & \boldsymbol{K}^{35}_L \\ & \boldsymbol{K}^{44}_L & \boldsymbol{K}^{45}_L \\ \text{sym} & & \boldsymbol{K}^{55}_L \end{bmatrix} \begin{Bmatrix} \boldsymbol{q}_w(t) \\ \boldsymbol{q}_{\phi_x}(t) \\ \boldsymbol{q}_{\phi_y}(t) \end{Bmatrix} = \boldsymbol{0} \quad (8)$$

Linear term $\boldsymbol{K}_{LS}^{33}$ and nonlinear term $\boldsymbol{K}_{NLS}^{33}(\boldsymbol{q}_w)$ can be found, for example, in Ref. [70]. In this study, the equations of motion of ROM1, represented by Eq. (8), have $3 \times 7^2 = 147$ DOFs.

C. ROM in Modal Coordinates

In the modal summation method employed here, the vibration is assumed to be given by a superposition of selected modes of conservative systems. In the absence of airflow and nonlinear terms, normal mode shapes are given by the eigenvectors $\boldsymbol{\phi}_i$ of $\lambda_i \boldsymbol{M}\boldsymbol{\phi}_i = \boldsymbol{K}_L\boldsymbol{\phi}_i$. Considering a reduced modal matrix $\boldsymbol{\Phi}$ composed of m normal mode shapes $\boldsymbol{\phi}_i$, the generalized displacements $\boldsymbol{q}$ can be related to modal displacements $\boldsymbol{q}_m$ by

$$\boldsymbol{q}(t) = \boldsymbol{\Phi}\boldsymbol{q}_m(t) \tag{9}$$

Premultiplying full-order equations (6) by the transpose of modal matrix, $\boldsymbol{\Phi}^T$, and substituting Eq. (9) in it, gives m modal equations of motion as

$$\bar{\boldsymbol{M}}\ddot{\boldsymbol{q}}_m(t) + \bar{\boldsymbol{F}}_{\text{unsteady}}\dot{\boldsymbol{q}}_m(t) + \left(\bar{\boldsymbol{K}}_L + \bar{\boldsymbol{K}}_{NL} + \bar{\boldsymbol{F}}_{\text{steady}}\right)\boldsymbol{q}_m(t) = \boldsymbol{0} \tag{10}$$

in which the modal mass matrix $\bar{\boldsymbol{M}}$ and the modal linear stiffness matrix $\bar{\boldsymbol{K}}_L$ are diagonal, but the modal nonlinear stiffness matrix $\bar{\boldsymbol{K}}_{NL}$ and the modal aerodynamics matrices $\bar{\boldsymbol{F}}_{\text{unsteady}}$ and $\bar{\boldsymbol{F}}_{\text{steady}}$ are not. Here, the system of ROM2 has m DOFs. In this paper, only the first 10 (lower-frequency) modes [76] are considered (so, $m = 10$). Again, it should be noted that, in Refs. [17–51], often six to eight modes were used.

D. Statically Condensed ROM in Modal Coordinates

In ROM3, the modal summation method is applied on a statically condensed model [ROM1 represented by Eq. (8)]. Normal modes are calculated from an already statically condensed linear problem, in which airflow velocity is equal to zero. The rest of the procedure is as explained in the previous section. The number of DOFs in ROM3 is also equal to the number of normal modes used (i.e., here, 10 DOFs).

III. Validation

Table 1 gives a comparison with a good agreement for the first five nondimensional linear natural frequencies ω_n of a moderately thick isotropic simply supported plate (with immovable edges) calculated by the present method (FOM; 245 DOFs), an FE with an inverse trigonometric shear deformation theory (ITSDT; Ref. [77]; 56 DOFs), an exact solution with three-dimensional (3-D) theory (Ref. [78]), and another exact solution with a higher-order shear deformation theory (HSDT; Ref. [79]). It is worthy to note that, because only bending modes exist in this table and because in-plane and out-of-plane terms are uncoupled in the linear regime, in-plane displacement components would not be needed. Thus, the number of DOFs of the FOM could be decreased to 147 DOFs. Aerodynamic pressure is not considered in this example.

Figure 2 compares LCO amplitudes of three simply supported (with immovable edges) composite laminates with configuration $[\theta, -\theta, \theta, -\theta, \theta]_{\text{sym}}$, in which $\theta = 0$, 30, and 60 deg, by the current method (FOM; 245 DOFs) and two references (Shiau and Lu [27] and Kouchakzadeh et al. [44]; both have FOMs with six DOFs). The CPT is used in Refs. [27,44]. The small difference between the results is due to the fact that neither the structural theories (TSDT vs CPT) nor the orders of the systems (245 DOFs vs 6 DOFs) are equal. This comparison verifies the correctness and exactness of the present method.

Table 1 Comparison of nondimensional linear frequencies ω_n of a simply supported isotropic square plate ($a/h = 10$; $\nu = 0.3$)

	Mode number				
Method	1	2	3	4	5
Present FOM (245 DOFs), TSDT	0.0930	0.2220	0.3406	0.4188	0.5235
FE (56 DOFs), ITSDT [77]	0.0931	0.2221	0.3409	0.4156	0.5215
Exact, 3-D theory [78]	0.0932	0.2226	0.3421	0.4171	0.5239
Exact, HSDT [79]	0.0931	0.2222	0.3411	0.4158	0.5221

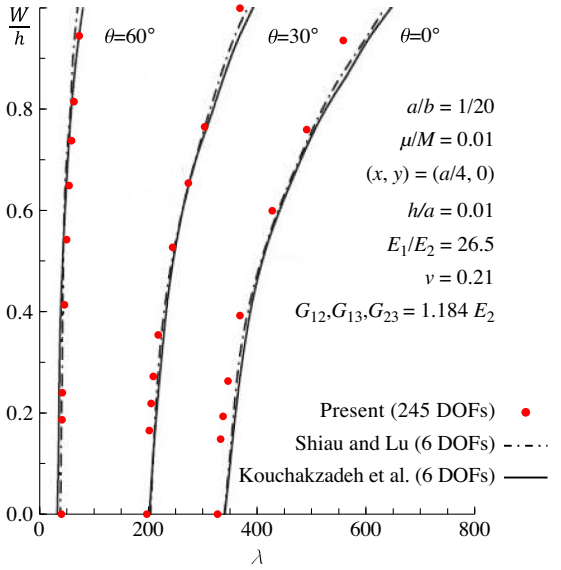

Fig. 2 Comparison of LCO amplitudes by the present and other methods.

Comparison and convergence examples performed in [21–32] are based on either ROMs or FOMs with a limited number of DOFs. Figures shown in those references imply that a converged ROM can still suffer from some approximation errors when compared with a converged FOM. In the next section, several analyses are carried out with the goal of finding how the mentioned approximation changes with various parameters.

IV. Results

In this study, a 12-layer laminate with fiber configurations $[\langle 45, 90\ \text{deg}\rangle, -\langle 45, 90\ \text{deg}\rangle, \langle 0, 45\ \text{deg}\rangle, -\langle 0, 45\ \text{deg}\rangle, \langle 90, 135\ \text{deg}\rangle, -\langle 90, 135\ \text{deg}\rangle]_{\text{sym}}$ is analyzed, in which the characteristic fiber angles of the first ply are $\langle T_0, T_1\rangle = \langle 45, 90\ \text{deg}\rangle$, the characteristic fiber angles of the second ply are $\langle T_0, T_1\rangle = -\langle 45, 90\ \text{deg}\rangle$, etc. The mechanical properties of the studied VSCL are as follows: $E_1 = 126.3$ and $E_2 = 8.765$, $G_{12} = G_{13} = 4.92$ and $G_{23} = 3.35$, $\nu_{12} = 0.334$, and $\rho = 1557$. These properties are supplied by the Netherlands Aerospace Centre [70] for some VSCLs manufactured there. Both h/a and μ/M are fixed at 0.01, except in Subsecs. IV.D–F, in which a moderately thick plate ($h/a = 0.1$) is considered and $\mu/M = 0.001$. The plates are square, $a/b = 1$, and all the layers have equal thickness. The airflow direction is parallel to the x coordinate. In this paper, if a cantilever plate is studied, then the edge $y = -b/2$ is fixed and the results are calculated at $(x, y) = (0, b/2)$; else, if a clamped or simply supported plate (with immovable edges in the in-plane surface) is analyzed, then the results are calculated at $(x, y) = (a/4, 0)$ (as represented in Fig. 3).

The relative errors, given in the tables of the current paper, measure the accuracy of the ROM approximations taking the FOM results as reference. The FOM generally has 245 physical DOFs of the p-version FE, ROM1 has 147 physical DOFs of the p-version FE, ROM2 has 10 DOFs coming from the first 10 normal modes of the FOM, and ROM3 has 10 DOF coming from the first 10 normal modes of ROM1. As pointed out, the number of modes is fixed at this relatively small number throughout the paper (unless otherwise stated) because this is the common procedure in the literature.

The final equations of the system, resulted from the FOM and ROMs, are solved using Newmark method with the time step equal to the system's fundamental linear period divided by 100. The length of the analysis is one million time steps equivalent to 10,000 times the system's fundamental linear period.

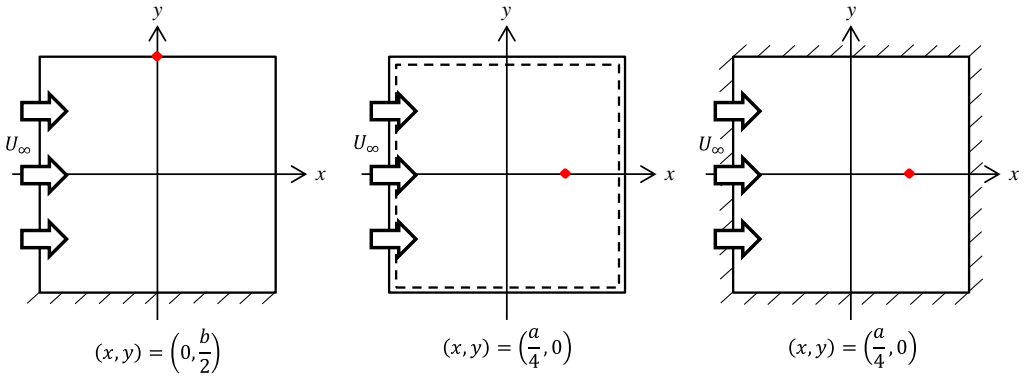

a) Cantilever plate **b) Simply-supported plate** **c) Clamped plate**

Fig. 3 Various boundary conditions and the point wherein the results are calculated.

A. Effect of Boundary Conditions

In this section, tables present the LCO amplitudes of the cantilever, simply supported, and clamped VSCL plates subjected to dynamic pressure until the amplitude of vibration displacement, at the points indicated in Fig. 3, reached around 1.2 times the plate thickness. In each table, the minimum dynamic pressure λ corresponds to the critical linear flutter pressure calculated by the linear FOM. In the reviewed references, often, researchers have considered simply supported boundary conditions, and only a few papers can be found on cantilever boundaries [17–23] or on clamped boundary conditions [31–36]. Researchers often considered more modes (or more DOF) in the cantilever-plate case than in the clamped-plate case. This shows that, normally, more DOF are required in the study of a cantilever plate, as it does not have symmetric boundary conditions.

1. *Cantilever Plate*

In the case of the cantilever plate (Table 2), the best approximations are from ROM1 (with 147 DOF). Between ROMs with 10 DOF, ROM3 is much better than ROM2. The error between the amplitudes of the ROMs and the FOM, in the largest deflection ratio, is −0.2, −94, and −4.1% for ROM1, ROM2, and ROM3, respectively. One may expect these approximations because, in this analysis, lower frequencies (so their normal modes) are associated with out-of-plane deflection and higher frequencies (so their normal modes) are connected with in-plane displacements. In the case of ROM2, the first 10 modes do not necessarily include in-plane modes. (In-plane and out-of-plane modes are uncoupled.) In the case of ROM3, coupling between in-plane and out-of-plane modes exists, and consequently, the first 10 modes include membrane effects. This explains the fact that, in this case, ROM3 gives a better approximation than ROM2. It is not unexpected that ROM2 leads to the worst approximation. It should be noted that ROM1 predicts the (critical) linear flutter at lower dynamic pressure, in comparison with the FOM, but ROM2 and ROM3 postpone the linear flutter to a higher dynamic pressure.

On the importance of in-plane modes, it is interesting to note that including some in-plane modes in the reduced modal matrix leads to a more exact ROM2. Naturally, a ROM2 with all normal modes should predict results equal to its associated FOM. To verify the modal reduction method implemented here, results by an FOM (exceptionally, in this comparison, with 80 DOF) are compared with those by ROM2, increasing the number of modes until convergence occurs (Table 3). A ROM2 with a large-enough number of modes (here, 50 modes or DOFs) predicts values equal to the ones of its associated FOM. However, the authors will, in this text, consider modal ROMs with a relatively small number of modes, because this is a common procedure in the literature, which, we believe, may lead to errors that have been ignored.

2. *Simply Supported Plate*

Although LCOs of the cantilever plate were periodic in the range of the studied parameters, in the case of the simply supported plate (Table 4), some oscillations by ROM2 became aperiodic (AP). Like in the case of the cantilever plate, ROM1 (147 DOF) predicts the closest amplitudes to the FOM amplitudes (0.1% in its maximum amplitude ratio), and ROM3 (with the error of 3.5%) acts better than ROM2 (both with 10 DOFs). LCOs predicted by ROM2, in this case, are often AP, whereas ROM1 and ROM3 predict periodic responses. By comparing the results of ROM2 for the cantilever and simply supported plates, one can see that the errors in the case of the simply supported plate are much smaller than what was seen in the cantilever plate. (For the cantilever plate, it was around 94%.) It is important to emphasize a defect of ROMs: in some cases where the FOM gives

Table 3 LCO amplitudes W/h of the cantilever VSCL; comparison between the FOM and ROM2

Model	DOF	W/h
FOM	80	1.151
ROM	10	0.066
— —	20	0.068
— —	30	0.094
— —	40	0.127
— —	50	1.151
— —	60	1.151

The dynamic pressure is fixed at $\lambda = 32.6$.

Table 2 LCO amplitudes W/h of the cantilever VSCL against different aerodynamic pressures

		λ									
Model	DOF (reduction)	33.59[a]	33.60	33.62	33.66	33.71	33.79	33.87	33.96	34.04	34.21
FOM	245	0.000	0.181	0.283	0.418	0.541	0.695	0.821	0.943	1.040	1.221
ROM1	147 (S[b])	0.063	0.181	0.283	0.417	0.540	0.694	0.819	0.941	1.037	1.218
Error, %		— —	−0.2	−0.2	−0.2	−0.2	−0.2	−0.2	−0.2	−0.2	−0.2
ROM2	10 (M[b])	0.000	0.000	0.000	0.014	0.026	0.038	0.047	0.055	0.061	0.073
Error, %		— —	−100	−100	−96.6	−95.2	−94.6	−94.3	−94.2	−94.1	−94.0
ROM3	10 (S, M)	0.000	0.000	0.000	0.226	0.413	0.601	0.743	0.877	0.980	1.171
Error, %		— —	−100	−100	−45.8	−23.8	−13.5	−9.4	−7.0	−5.7	−4.1

[a]Linear flutter dynamic pressure calculated by the FOM.

[b]M and S identify modal summation technique and static condensation technique, respectively.

Table 4 LCO amplitudes W/h of the simply supported VSCL against different aerodynamic pressures

		λ									
Model	DOF (reduction)	144	146	150	168	187	207	229	251	274	299
FOM	245	0.000	0.138	0.242	0.488	0.653	0.774	0.969	1.020	1.080	1.253
ROM1	147 (S)	0.000	0.140	0.243	0.489	0.654	0.775	0.970	1.019	AP	1.254
Error, %		— —	1.4	0.5	0.2	0.1	0.1	0.1	−0.1	— —	0.1
ROM2	10 (M)	0.101	0.159	0.237	0.455	0.613	AP	AP	0.858	AP	AP
Error, %		— —	15.0	−2.0	−6.8	−6.1	— —	— —	−15.9	— —	— —
ROM3	10 (S, M)	0.118	0.185	0.274	0.513	0.678	0.802	1.012	1.101	1.196	97
Error, %		— —	34.1	13.4	5.0	3.9	3.6	4.4	7.9	10.8	3.5

Table 5 LCO amplitudes W/h of the clamped VSCL against different aerodynamic pressures (FOM; 245 DOF)

λ	W/h
1645	AP
1655	AP
1670	0.067[a,b]
1685	0.092
1700	AP
1730	AP
1760	AP
1790	AP[b]
1830	AP[a,b]
1885	1.301[b]

[a]Time histories, phase-plane plots, and Poincaré sections of these cases are depicted in Fig. 4.

[b]In these cases, the maximum Lyapunov exponent and the FFT of the time history are shown in Figs. 5 and 6.

periodic oscillations, some ROMs (specifically, ROM1 and ROM2) predict AP oscillations. In what concerns linear flutter predictions, all three ROMs predicted a critical dynamic pressure lower than that of the FOM (i.e., $\lambda = 144$).

3. Clamped Plate

Table 5 tabulates the amplitudes of the LCOs calculated by the FOM for the clamped VSCL plate. In comparison with the simply supported and cantilever plates, AP oscillations happen more often in the clamped plate. In this case, vibrations are periodic in few LCO amplitudes, and they lose easily their periodicity with a change in aerodynamic pressure. Because most of the results predicted by the FOM, here, are AP, associated results by the ROMs are not presented.

AP motions, observed in the case of clamped boundaries, restrain the use of ROMs. Some references (e.g., [36]) have mentioned a chaotic behavior for plates under supersonic airflow. In this case, the claim was supported only by checking the time histories of the oscillations. To prove that these oscillations are chaotic, one should not only inspect their time histories, phase-plane plots, and Poincaré sections, but also compute their Lyapunov exponents.

Time histories, phase-plane plots, and Poincaré sections of a periodic and an apparently AP solution in Table 5, with $\lambda = 1670$ and $\lambda = 1830$, are depicted in Fig. 4. Time-history plots display transient motion until the steady-state motion is reached; phase-plane plots and Poincaré sections are shown for steady-state motion. To define the Poincaré sections of the AP solution, because there is not any external excitation period, we decided to collect points from the phase-plane plots at instants separated by the first linear natural period of vibration of the plate subjected to airflow.

To verify if some irregular oscillations are indeed chaotic, an algorithm, written in FORTRAN (appendix B of [80]), was applied to determine the maximum Lyapunov exponent from a time series. The results are shown in Fig. 5 for four vibration motions given in Table 5 (i.e., $\lambda = 1670$, 1790, 1830, and 1885). Another important and supportive tool to achieve a better understanding on the nature of oscillations is Fourier spectrum, which can be computed via fast Fourier transform (FFT). Figure 6 depicts Fourier spectra of oscillations at the mentioned dynamic pressures. In the case of $\lambda = 1790$, the maximum Lyapunov exponent is positive, and one can note that a broadband character exists around a few frequencies in the spectrum; this oscillation is chaotic. When the dynamic pressure is $\lambda = 1670$ or $\lambda = 1885$, the maximum Lyapunov exponent converges to zero or, apparently, to a negative value that is close to zero, and the spectrum consists of a single discrete peak, identifying a periodic LCO, in which one harmonic dominates. If $\lambda = 1830$, the phase-plane plot appears to be a closed line, but a zoom shows that the line is not exactly closing. In this case, the maximum Lyapunov exponent also converges to zero, but the spectrum of this oscillation is dominated by three discrete frequencies, which do not appear to be related by integers. If the latter two features are true, then this motion is quasi-periodic. Finally, it should be noted that, because there is no in-plane or thermal loading in the current study, these AP behaviors differ from chaotic motions of plates simultaneously subjected to flow pressure and in-plane compressive loading (found, e.g., in Refs. [28–31,33]).

B. Effect of Viscous Damping

Viscous damping, represented by a matrix proportional to the linear stiffness matrix ($\alpha \boldsymbol{K}_L$), which multiplies by vector $\dot{\boldsymbol{q}}$ in FOM and ROM1, and by vector $\dot{\boldsymbol{q}}_m$ in ROM2 and ROM3, is added to the models. The coefficient of viscous damping α is extracted from experiments [81] and is equal to 6.36×10^{-5}. Usually, researchers did not include viscous damping in the nonlinear flutter analysis of plates [17–51]. However, it has been found in Refs. [82–87] that the plate can be made unstable through the addition of damping to the equations. This "destabilizing effect" is commonly said to occur when viscous or structural damping interacts to reduce the effect of aerodynamic damping in a multi-DOF nonconservative system [82,83].

Table 6 gives the LCO amplitudes of the cantilever VSCL plate when viscous damping is included in the equations. This table can be compared with Table 2, in which the same plate without viscous damping is tested. Table 6 shows that, according to the FOM, the oscillations of the plate with viscous damping become unstable and the associated amplitudes markedly grow, eventually until a new limit cycle is attained. This happens when the dynamic pressure is larger than about 33.70. Meanwhile, the ROMs could not predict this loss of stability and continued to predict low-amplitude LCOs (i.e., an important disadvantage of using such ROMs in plates in which viscous damping is included). Because ROMs suppressed or postponed stability losses, the errors between the FOM and ROMs are very large, and they are not shown in this table. As written in the preceding paragraph, when the low-amplitude (weak) LCOs loose stability, the oscillations may converge to a large-amplitude (strong) LCO. In the studied cases, the amplitude of the new LCO was very high (around 10 times the plate thickness); hence, the von Kármán and linear-elastic-type model adopted here probably does not apply. Nonetheless, for illustration purposes, a steady-state time-history plot and phase-plane plot for such LCO at $\lambda = 33.70$ are depicted in Fig. 7.

To clarify the source of such destabilization, Fig. 8 presents the LCO amplitudes of the cantilever VSCL plate against dynamic pressures, computed by the FOM, with and without viscous damping parameter. In Fig. 8a, in which viscous damping is not

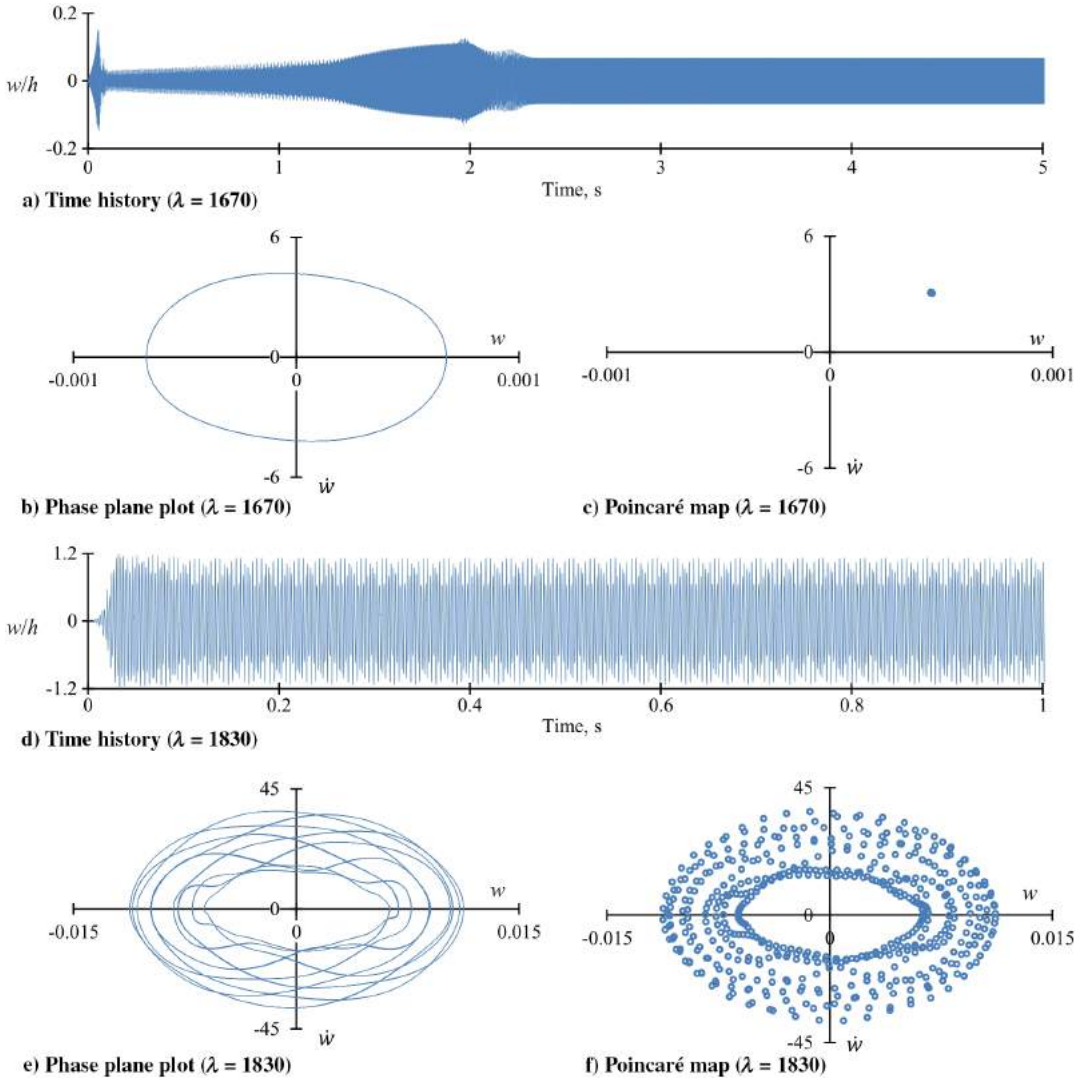

Fig. 4 Periodic and AP oscillation for the clamped VSCL under various dynamic pressures.

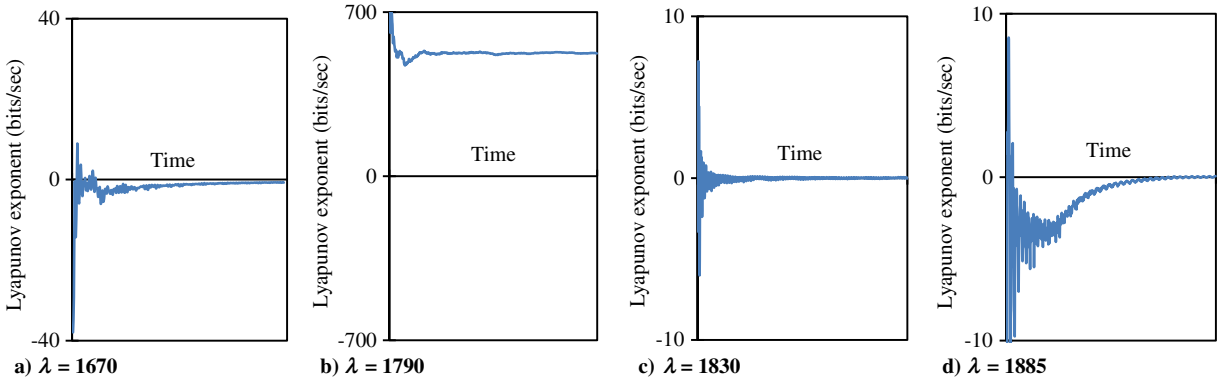

Fig. 5 Maximum Lyapunov exponents against time for the VSCL under various dynamic pressures.

considered, the LCO is benign [71]; this subfigure repeats data from Table 2, but it is presented here to facilitate the comparison. Here, a perturbation below the linear critical flutter boundary leads to a stable static equilibrium (zone 1), and any perturbation beyond the linear critical flutter boundary results in a stable LCO (zone 2). In Fig. 8b, in which the effect of viscous damping is included, four scenarios are detected and the strongest LCO is detrimental [71]. Here, a perturbation in zone 1 leads to a stable static equilibrium. In zone 2, a small perturbation leads to a stable static equilibrium, but a large perturbation results in a large-amplitude (strong) LCO. In zone 3, a small and large perturbation result in, respectively, a low-amplitude (weak) LCO and a large-amplitude (strong) LCO. In zone 4, any perturbation leads to a strong LCO. As already noted, the large-amplitude LCOs are quite probably not exact, because their amplitudes are around 10 times the thickness, and consequently, von Kármán model is not valid. Furthermore, a catastrophic failure may occur before such large amplitude is reached.

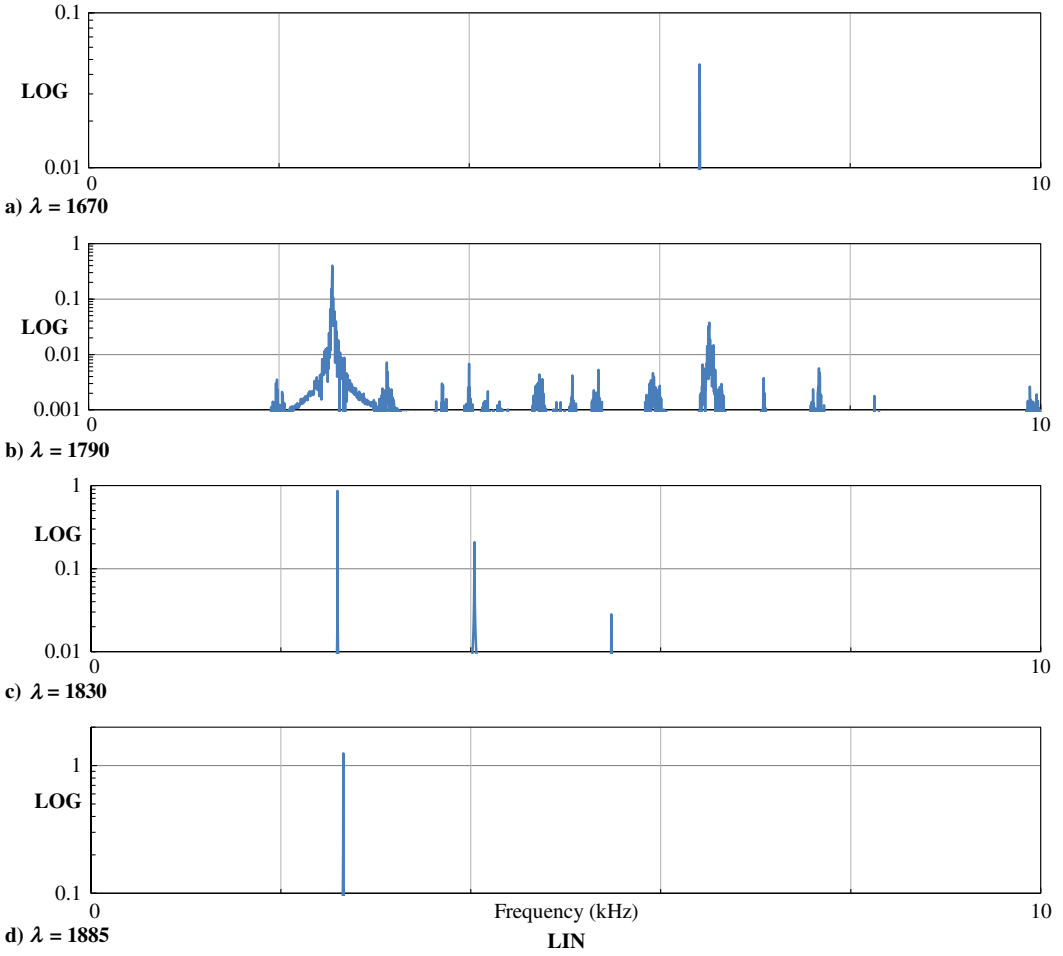

Fig. 6 Frequency spectra of responses of the VSCL under various dynamic pressures.

C. Effect of Geometric Imperfection

In the references reviewed by the authors [17–51], no study was found on the accuracy of ROMs in the nonlinear flutter of imperfect plates. The amplitudes of LCOs of an imperfect VSCL plate computed using the FOM and the ROMs are shown in Table 7. The imperfection has the shape of a half-sine wave, a stress-free "initial deflection" with respect to the flat plate, given by $h_i \cos(\pi x/a)\cos(\pi y/b)$. LCO amplitudes and aerodynamic pressures of the cantilever, imperfect ($h_i = h$), VSCL plate, in Table 7, can be compared with those of the corresponding perfect ($h_i = 0$) plate in Table 2. Because of the imperfection, the aerodynamic pressure at which flutter appears significantly decreases. The comparison between both tables shows that the errors due to using ROM2 and ROM3 are smaller in the case of imperfect plates. The reduction in the error of these approximations is probably due to the coupling between transverse and membrane displacement components that is introduced by the transverse imperfection, leading to lower-order linear modes of vibration that include not only transverse, but also membrane terms. In the case of ROM3, the error for the perfect plate was at least 4.1% (Table 2), whereas the minimum value in the imperfect plate case is 0.8% (Table 7). Errors by ROM1 slightly increased in the imperfect plate; because this reduction technique does not use normal modes, it does not benefit from the aforementioned coupling.

D. Effect of Laminate Thickness

A few publications consider nonlinear flutter of moderately thick plates; Refs. [22,23,33,35] used FSDT, and a TSDT is applied in Ref. [18]. In these references, ROMs with a small number (from 2 to 16) of modes are used. Furthermore, Refs. [18,35] applied static condensation. Because the number of works on moderately thick plates is not large and apparently ROMs were always employed, it seems important to evaluate the accuracy of ROMs to analyze nonlinear flutter of thick plates. Table 8 gives the LCO amplitudes for the cantilever, moderately thick ($h/a = 0.1$), VSCL plate subjected to increasing dynamic pressure. This table can be compared with Table 2, in which a similar, but thin ($h/a = 0.01$), plate was

Table 6 LCO amplitudes W/h of the cantilever VSCL against different aerodynamic pressures, in which the viscous damping parameter is included in the models

		λ									
Model	DOF (reduction)	33.56	33.57	33.58	33.59	33.60	33.62	33.65	33.70	33.80	33.90
FOM	245	0.000[a]	0.154[a]	0.257[a]	0.336[a]	0.406[a]	0.536[a]	0.784[a]	DS[b]	DS	DS
ROM1	147 (S)	0.000	0.117	0.193	0.249	0.294	0.368	0.457	0.576	0.761	0.909
ROM2	10 (M)	0.000	0.000	0.000	0.000	0.000	0.005	0.018	0.028	0.042	0.052
ROM3	10 (S, M)	0.000	0.000	0.000	0.000	0.000	0.087	0.286	0.454	0.674	0.839

[a]Amplitudes of the low-amplitude (weak) LCO.

[b]DS identifies a solution of weak LCO that loses its stability, and it grows to a large-amplitude (strong) LCO. The steady-state time history and phase-plane plot of the strong LCO are given in Fig. 7.

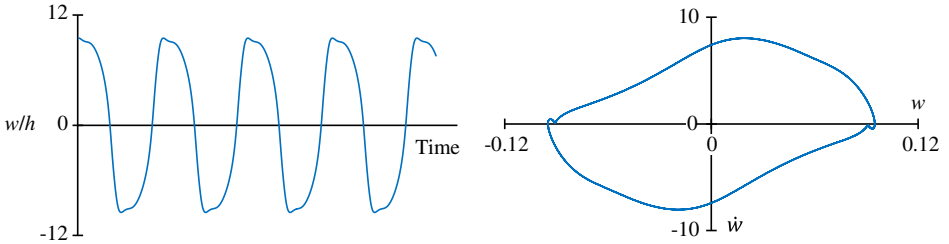

a) Steady state time history **b) Phase plane plot**

Fig. 7 Large-amplitude LCO of the VSCL with viscous damping.

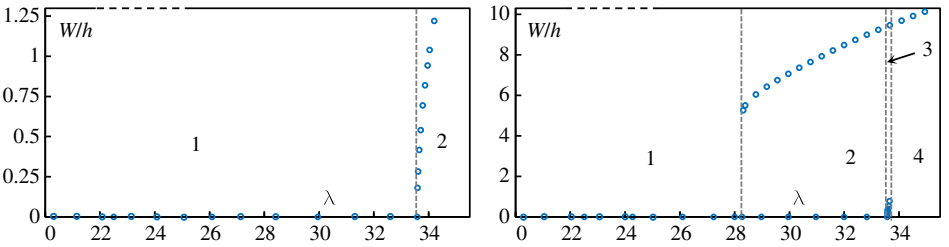

a) Viscous damping excluded **b) Viscous damping included**

Fig. 8 Effect of viscous damping on LCO amplitudes of the VSCL.

evaluated. A comparison between the two tables shows an increased inaccuracy of the ROMs for moderately thick plates. In the moderately thick plate, the nearest results to the FOM are from the statically condensed model with 147 DOF (ROM1), in which the approximation error is at least 13%, as a result of the larger importance of membrane inertia. It is also interesting to note that, although no AP motion was seen in the thin-plate case (Table 2), in the moderately thick plate under dynamic pressure $\lambda = 21.69$, the motion predicted by the FOM is AP (Table 8).

E. Approximations in Stresses

Especially when ROMs have been applied, attention has not been paid in the literature to the stresses that develop when plates experience nonlinear flutter. Hence, it is appropriate to examine the efficiency of ROMs in the calculation of stresses. Having accurate-enough stresses by ROMs is important to detect failure onset by stress-based failure criteria or to estimate fatigue life. Figure 9 displays the in-plane normal and in-plane shear stresses (i.e., σ_x, σ_y, τ_{xy}) and transverse shear stresses calculated by constitutive relations, with superscript c, and by equilibrium equations of 3-D elasticity, with superscript e (i.e., $\tau_{xz}^{(c)}$, $\tau_{yz}^{(c)}$, $\tau_{xz}^{(e)}$, $\tau_{yz}^{(e)}$) for the LCO of the cantilever VSCL plate. For this analysis, the moderately thick plate ($h/a = 0.1$) is under aerodynamic pressure, $\lambda = 21.40$ (case taken from Table 8). Because in-plane stresses are close to zero at the midplane of the plate, they are calculated at the top surface and edge of the plate, in which $(x, y, z) = (a/2, 0, h/2)$. Transverse shear stresses are close to zero on the surfaces; hence, they are calculated at the midplane and edge of the plate, in which $(x, y, z) = (a/2, 0, 0)$. The stresses displayed in Fig. 9 are calculated for an oscillation cycle at the steady-state motion of the plate. This figure confirms that both ROM1 and ROM3 provide more accurate stresses than ROM2. In the case of transverse shear stresses, calculated by equilibrium equations of 3-D elasticity, ROM1 and ROM3 predict stress histories, which show higher harmonics, but the stress history by the FOM displays a simple harmonic. More often than not, all ROMs led to inaccurate stress computations.

Table 7 LCO amplitudes W/h of the cantilever imperfect VSCL against different aerodynamic pressures

		λ									
Model	DOF (reduction)	21.41	21.43	21.49	21.56	21.66	21.76	21.89	22.06	22.23	22.57
FOM	245	0.000	0.145	0.308	0.429	0.562	0.671	0.794	0.932	1.054	1.268
ROM1	147 (S)	0.000	0.110	0.292	0.418	0.553	0.663	0.786	0.925	1.048	1.262
Error, %		— —	−24.0	−5.2	−2.8	−1.7	−1.3	−1.0	−0.7	−0.6	−0.5
ROM2	10 (M)	0.000	0.011	0.034	0.048	0.063	0.075	0.089	0.104	0.117	0.140
Error, %		— —	−92.6	−89.1	−88.8	−88.8	−88.8	−88.8	−88.9	−88.9	−89.0
ROM3	10 (S, M)	0.000	0.002	0.271	0.403	0.541	0.654	0.778	0.919	1.043	1.258
Error, %		— —	−98.5	−12.2	−6.2	−3.7	−2.6	−1.9	−1.4	−1.1	−0.8

Table 8 LCO amplitudes W/h of the cantilever moderately thick VSCL against different aerodynamic pressures

		λ									
Model	DOF (reduction)	21.29	21.30	21.32	21.35	21.40[a]	21.43	21.45	21.53	21.61	21.69
FOM	245	0.000	0.106	0.277	0.418	0.582	0.661	0.708	0.875	1.016	AP
ROM1	147 (S)	0.000	0.092	0.239	0.361	0.503	0.572	0.614	0.759	0.881	0.990
Error, %		— —	−13.7	−13.7	−13.5	−13.4	−13.4	−13.3	−13.3	−13.3	— —
ROM2	10 (M)	0.000	0.000	0.000	0.012	0.030	0.037	0.041	0.053	0.064	0.073
Error, %		— —	−100	−100	−97.1	−94.8	−94.4	−94.3	−93.9	−93.7	— —
ROM3	10 (S, M)	0.000	0.000	0.000	0.139	0.378	0.467	0.517	0.684	0.818	0.934
Error, %		— —	−100	−100	−66.8	−34.9	−29.3	−27.0	−21.8	−19.5	— —

[a]Stresses for this VSCL plate are displayed in Fig. 9.

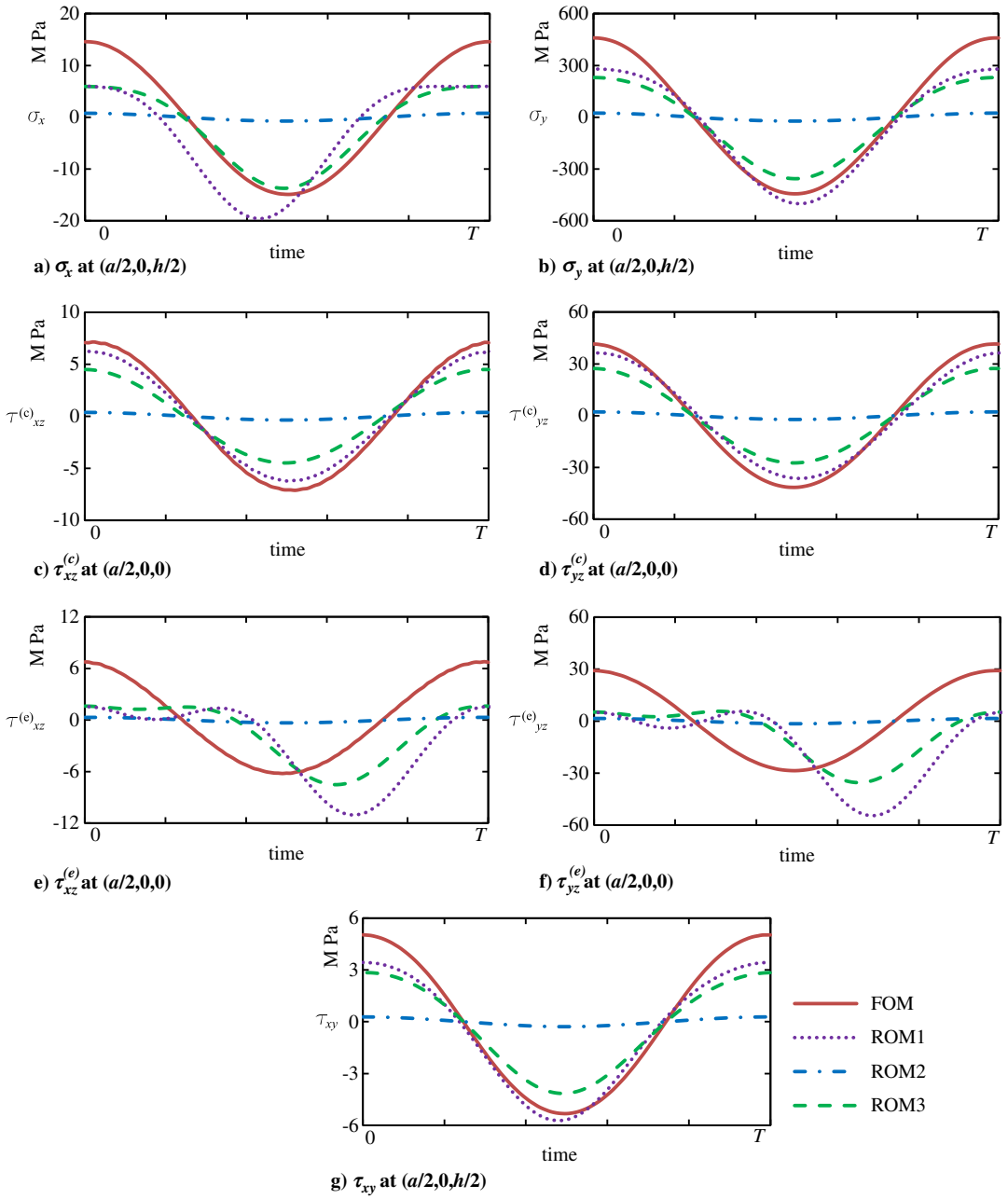

Fig. 9 Stresses in the moderately thick cantilever VSCL under aerodynamic pressure $\lambda = 21.40$.

F. Approximations in Damage Criterion Index

Also in what failure analysis is concerned, no attention has been paid to the efficiency of ROMs in nonlinear flutter of plates. In this section, a quadratic, interactive Tsai–Wu failure criterion, taking into consideration a multi-axial stress state and how the combination of different stress components affects the damage onset [88], is used. Accordingly, damage starts when the damage index is greater than or equal to 1. The damage criterion index is calculated using stresses in material coordinates by

$$\text{Damage index} = \frac{1}{X_t X_c}\sigma_1^2 + \frac{1}{Y_t Y_c}(\sigma_2^2 + \sigma_3^2) + \frac{1}{S_{12}^2}(\tau_{12}^2 + \tau_{13}^2) + \frac{1}{S_{23}^2}(\tau_{23}^2 - \sigma_2\sigma_3) + \left(\frac{1}{X_t} - \frac{1}{X_c}\right)\sigma_1 + \left(\frac{1}{Y_t} - \frac{1}{Y_c}\right)(\sigma_2 + \sigma_3) + \frac{2 \times -0.5}{\sqrt{X_t X_c Y_t Y_c}}\sigma_1(\sigma_2 + \sigma_3) \tag{11}$$

in which $X_t = 2280$, $X_c = 1440$, $Y_t = 57$, $Y_c = 228$, and $S = 71$ (provided by the Netherlands Aerospace Centre [70] for some VSCLs manufactured there). Here, σ and τ are stresses in material coordinates (1, 2, and 3). Table 9 gives the Tsai–Wu damage index of the moderately thick cantilever VSCL plate ($h/a = 0.1$) with the increase of dynamic pressure. The LCO amplitudes of this plate were given in Table 8. Table 9 also gives the location of the maximum damage index in the plate. This table shows that, according to the FOM, damage already started in the VSCL plates under dynamic pressure lower than $\lambda = 21.40$. (Thus, the validity of the results presented at higher dynamic pressures is questionable.) ROM2 provides the worst predictions of damage onset, whereas the results of ROM1 are closest to the FOM. In comparison with the FOM, all three ROMs postpone prediction of the damage onset, to higher dynamic pressures. Although all three ROMs predict similar position for the maximum damage index (on the fixed edge of the cantilever plate), the FOM prediction for the location of the maximum damage is different.

Table 9 Maximum Tsai–Wu damage index as well as its position [$x/(a/2)$, $y/(b/2)$, $z/(h/2)$] in the cantilever VSCL against different aerodynamic pressures

		λ									
Model	DOF (reduction)	21.29	21.30	21.32	21.35	21.40	21.43	21.45	21.53	21.61	21.69
FOM	245	0.000	0.126	0.370	0.646	1.043	1.266	1.412	1.985	2.556	AP[a]
Position		— —	1, −1, 3/100	1, −1, −3/100	1, −7/10, 5/100	1, −7/10, 5/100	1, −7/10, −5/100	1, −75/100, 5/100	1, −75/100, 5	1, −75/100, −5/100	— —
ROM1	147 (*S*)	0.006	0.109	0.329	0.556	0.877	1.056	1.174	1.634	2.091	2.553
Position		−1, −1, 3/100	1, −1, 3/100	1, −1, −3/100	1, −1, −3/100	1, −1, 3/100	1, −1, −3/100	1, −1, −3/100	1, −1, 3/100	1, −1, −3/100	1, −1, 3/100
Error, %		— —	−13	−11	−14	−16	−17	−17	−18	−18	— —
ROM2	10 (*M*)	0.000	0.000	0.000	0.013	0.034	0.042	0.047	0.062	0.075	0.087
Position		— —	— —	— —	1, −1, 3/100	1, −1, 3/100	1, −1, 3/100	1, −1, −3/100	1, −1, −3/100	1, −1, 3/100	1, −1, −3/100
Error, %		— —	−100	−100	−98	−97	−97	−97	−97	−97	— —
ROM3	10 (*S*, *M*)	0.000	0.000	0.000	0.174	0.592	0.789	0.914	1.390	1.854	2.319
Position		— —	— —	— —	1, −1, −3/100	1, −1, −3/100	1, −1, 3/100	1, −1, 3/100	1, −1, −3/100	1, −1, −3/100	1, −1, −3/100
Error, %		— —	−100	−100	−73	−43	−38	−35	−30	−27	— —

[a]The solution is AP.

V. Conclusions

A rectangular variable-stiffness composite laminate (VSCL) was modeled by a *p*-version FE and using a third-order shear deformation theory. The fibers in the composite plate had curvilinear paths, with a fiber orientation angle changing linearly from one vertical edge to the other vertical edge. Aerodynamic pressure due to a supersonic airflow modeled by the linear piston theory was applied to the structure model, and then equations of motion were obtained using the principle of virtual work (resulting in a model named full-order model (FOM)).

Three reduced-order models (ROMs) based on static condensation and the modal summation method were formed, and their results were compared with the FOM. Approximation errors due to using ROMs instead of the FOM were quantified. It was shown that using modal ROMs with a relatively small number of modes, a common practice in the literature, leads to errors that have been overlooked. The following conclusions were taken for VSCL plates under aerodynamic pressure:

1) Boundary conditions: change of boundary conditions can result in the appearance of aperiodic oscillations; in such boundary conditions, ROMs can wrongly lead to chaotic oscillations, whereas the FOM predicts a periodic motion;

2) Consideration of viscous damping: inclusion of viscous damping in the equations caused solutions of the FOM to lose stability after a certain limit-cycle oscillation (LCO) amplitude, leading to higher-amplitude LCOs; ROMs could not predict this loss of stability;

3) Plate thickness: it was verified that the considered ROMs could not precisely predict the correct behavior of moderately thick plates, with accuracy decreasing as the thickness increases;

4) Imperfection: ROMs generally led to better approximations when the plates were imperfect than when they were perfect;

5) Stresses: prediction of stresses by the mentioned ROMs was, in some cases, acceptable, but always with nonnegligible errors; the ROM with modal coordinates (ROM2) led to a quite deficient stress calculation;

6) Damage: prediction of damage onset by the ROMs was not satisfactory; in particular, none of the ROMs could predict the position of the maximum damage index as the FOM did.

In conclusion, whenever stress and damage were concerned, all the ROMs performed badly. If deflection was monitored, then it was shown that

1) FOM has the most exact results, but it has the highest computational cost;

2) ROM1 has the closest results to the FOM, but its computational cost is only slightly lower than the one of FOM;

3) ROM2 has the worst results, but it is as fast as ROM3;

4) ROM3 often leads to more acceptable deflection results than ROM2, and it also has the lowest computational cost (similar to ROM2).

Regarding ROM2, the weakness comes from the fact that the first modes do not necessarily include in-plane modes (if the plate is perfect, in-plane and out-of-plane modes are uncoupled in ROM2). In ROM3, coupling between in-plane and out-of-plane modes exists, and consequently, the first modes include membrane effects. This explains why approximations by ROM3 are better than by ROM2, when both approaches have the same number of degrees of freedom (DOFs). Naturally, the results of ROM2 and ROM3 should converge, respectively, to the results of FOM and ROM1 as more modes are taken into consideration. The results by ROM1 cannot converge more, because it has the maximum number of DOF it can have. If it is true that ROMs can be improved by using more DOF/modes, it is important to precisely select the modes to employ. However, this is a difficult choice.

The authors would end by remembering—as mentioned in the Introduction section—that, although they focused on ROMs based on static condensation and on structural modes of vibration, other methods, like employing aeroelastic modes instead of structural ones or resorting to proper orthogonal decomposition, exist.

Acknowledgments

The authors gratefully acknowledge the funding of Project NORTE-01-0145-FEDER-000022 SciTech—Science and Technology for Competitive and Sustainable Industries, cofinanced by Programa Operacional Regional do Norte (NORTE 2020), through Fundo Europeu de Desenvolvimento Regional. The authors would also like to thank Vasily Vedeneev, from Lomonosov Moscow State University, for valuable discussions.

References

[1] Thompson, J. M. T., and Stewart, H. B., *Nonlinear Dynamics and Chaos*, Wiley, West Sussex, England, 2002, Chap. 4.

[2] Lukaszewicz, D. H. J. A., Ward, C., and Potter, K. D., "The Engineering Aspects of Automated Prepreg Layup: History, Present and Future," *Composites Part B: Engineering*, Vol. 43, No. 3, 2012, pp. 997–1009. doi:10.1016/j.compositesb.2011.12.003

[3] Ungwattanapanit, T., and Baier, H., "Postbuckling Analysis and Optimization of Stiffened Fuselage Panels Utilizing Variable-Stiffness Laminates," *Proceedings of the 29th Congress of the International Council of the Aeronautical Sciences (ICAS2014)*, ICAS, Stockholm, Sweden, 2014, p. 2321.

[4] Mignolet, M. P., Przekop, A., Rizzi, S. A., and Spottswood, S. M., "A Review of Indirect/Non-Intrusive Reduced Order Modeling of Nonlinear Geometric Structures," *Journal of Sound and Vibration*, Vol. 332, No. 10, 2013, pp. 2437–2460. doi:10.1016/j.jsv.2012.10.017

[5] Przekop, A., and Rizzi, S. A., "Dynamic Snap-Through of Thin-Walled Structures by a Reduced-Order Method," *AIAA Journal*, Vol. 45, No. 10, 2007, pp. 2510–2519. doi:10.2514/1.26351

[6] Przekop, A., Guo, X., and Rizzi, S. A., "Alternative Modal Basis Selection Procedures for Reduced-Order Nonlinear Random Response Simulation," *Journal of Sound and Vibration*, Vol. 331, No. 17, 2012, pp. 4005–4024. doi:10.1016/j.jsv.2012.03.034

[7] Rizzi, S. A., and Przekop, A., "System Identification-Guided Basis Selection for Reduced-Order Nonlinear Response Analysis," *Journal of Sound and Vibration*, Vol. 315, No. 3, 2008, pp. 467–485. doi:10.1016/j.jsv.2007.12.031

[8] Gai, G., and Timme, S., "Nonlinear Reduced-Order Modelling for Limit-Cycle Oscillation Analysis," *Nonlinear Dynamics*, Vol. 84, No. 2, 2016, pp. 991–1009. doi:10.1007/s11071-015-2544-9

[9] Gang, C., Yingtao, Z., Jian, S., and Yueming, L., "Support-Vector-Machine-Based Reduced-Order Model for Limit Cycle Oscillation Prediction of Nonlinear Aeroelastic System," *Mathematical Problems in Engineering*, Vol. 2012, 2012, Article 152123. doi:10.1155/2012/439805

[10] Gang, C., Yueming, L., and Guirong, Y., "Active Control Law Design for Flutter/LCO Suppression Based on Reduced Order Model Method," *Chinese Journal of Aeronautics*, Vol. 23, No. 6, 2010, pp. 639–646. doi:10.1016/S1000-9361(09)60265-X

[11] Balajewicz, M., and Dowell, E., "Reduced-Order Modeling of Flutter and Limit-Cycle Oscillations Using the Sparse Volterra Series," *Journal of Aircraft*, Vol. 49, No. 6, 2012, pp. 1803–1812. doi:10.2514/1.C031637

[12] Zhang, W., Wang, B., and Ye, Z., "High Efficient Numerical Method for Limit Cycle Flutter Analysis Based on Nonlinear Aerodynamic Reduced-Order-Model," *51st AIAA/ASME/ASCE/AHS/ASC Structures, Structural Dynamics, and Materials Conference*, AIAA Paper 2010-2723, April 2010. doi:10.2514/6.2010-2723

[13] Da Ronch, A., Badcock, K., Wang, Y., Wynn, A., and Palacios, R., "Nonlinear Model Reduction for Flexible Aircraft Control Design," *AIAA Atmospheric Flight Mechanics Conference*, AIAA Paper 2012-4404, Aug. 2012. doi:10.2514/6.2012-4404

[14] Chen, G., Li, D., Zhou, Q., Da Ronch, A., and Li, Y., "Efficient Aeroelastic Reduced Order Model with Global Structural Modifications," *Aerospace Science and Technology*, Vol. 76, May 2018, pp. 1–13. doi:10.1016/j.ast.2018.01.023

[15] Zhou, Q., Li, D.-f., Da Ronch, A., Chen, G., and Li, Y.-m., "Computational Fluid Dynamics-Based Transonic Flutter Suppression with Control Delay," *Journal of Fluids and Structures*, Vol. 66, Oct. 2016, pp. 183–206. doi:10.1016/j.jfluidstructs.2016.07.002

[16] Badcock, K. J., Timme, S., Marques, S., Khodaparast, H., Prandina, M., Mottershead, J., Swift, A., Da Ronch, A., and Woodgate, M., "Transonic Aeroelastic Simulation for Instability Searches and Uncertainty Analysis," *Progress in Aerospace Sciences*, Vol. 47, No. 5, 2011, pp. 392–423. doi:10.1016/j.paerosci.2011.05.002

[17] Young, T. H., and Chen, F. Y., "Non-Linear Vibration of Cantilever Skew Plates Subjected to Aerodynamic and In-Plane Exciting Forces," *Journal of Sound and Vibration*, Vol. 182, No. 3, 1995, pp. 427–440. doi:10.1006/jsvi.1995.0209

[18] Zhao, M. H., and Zhang, W., "Nonlinear Dynamics of Composite Laminated Cantilever Rectangular Plate Subject to Third-Order Piston Aerodynamics," *Acta Mechanica*, Vol. 225, No. 7, 2014, pp. 1985–2004. doi:10.1007/s00707-013-1035-7

[19] Xie, D., and Xu, M., "A Comparison of Numerical and Semi-Analytical Proper Orthogonal Decomposition Methods for a Fluttering Plate," *Nonlinear Dynamics*, Vol. 79, No. 3, 2015, pp. 1971–1989. doi:10.1007/s11071-014-1787-1

[20] Stanford, B., and Beran, P., "Computational Strategies for Reliability-Based Structural Optimization of Aeroelastic Limit Cycle Oscillations," *Structural and Multidisciplinary Optimization*, Vol. 45, No. 1, 2012, pp. 83–99. doi:10.1007/s00158-011-0663-6

[21] Dowell, E., and Ye, W., "Limit Cycle Oscillation of a Fluttering Cantilever Plate," *AIAA Journal*, Vol. 29, No. 11, 1991, pp. 1929–1936. doi:10.2514/3.10821

[22] Farhadi, S., and Hosseini-Hashemi, S., "Aeroelastic Behavior of Cantilevered Rotating Rectangular Plates," *International Journal of Mechanical Sciences*, Vol. 53, No. 4, 2011, pp. 316–328. doi:10.1016/j.ijmecsci.2011.01.013

[23] Ghadimi, M., Dardel, M., Pashaei, M. H., and Barzegari, M. M., "Effects of Geometric Imperfections on the Aeroelastic Behavior of Functionally Graded Wings in Supersonic Flow," *Aerospace Science and Technology*, Vol. 23, No. 1, 2012, pp. 492–504. doi:10.1016/j.ast.2011.10.007

[24] Dowell, E. H., "Nonlinear Oscillations of a Fluttering Plate," *AIAA Journal*, Vol. 4, No. 7, 1966, pp. 1267–1275. doi:10.2514/3.3658

[25] Epureanu, B. I., Tang, L. S., and Padoussis, M. P., "Coherent Structures and Their Influence on the Dynamics of Aeroelastic Panels," *International Journal of Non-Linear Mechanics*, Vol. 39, No. 6, 2004, pp. 977–991. doi:10.1016/S0020-7462(03)00090-8

[26] Haddadpour, H., Navazi, H. M., and Shadmehri, F., "Nonlinear Oscillations of a Fluttering Functionally Graded Plate," *Composite Structures*, Vol. 79, No. 2, 2007, pp. 242–250. doi:10.1016/j.compstruct.2006.01.006

[27] Shiau, L. C., and Lu, L. T., "Nonlinear Flutter of Two-Dimensional Simply Supported Symmetric Composite Laminated Plates," *Journal of Aircraft*, Vol. 29, No. 1, 1992, pp. 140–145. doi:10.2514/3.46137

[28] Xue, D. Y., and Mei, C., "Finite Element Nonlinear Flutter and Fatigue Life of Two-Dimensional Panels with Temperature Effects," *Journal of Aircraft*, Vol. 30, No. 6, 1993, pp. 993–1000. doi:10.2514/3.46444

[29] Rezaee, M., and Jahangiri, R., "Nonlinear and Chaotic Vibration and Stability Analysis of an Aero-Elastic Piezoelectric FG Plate Under Parametric and Primary Excitations," *Journal of Sound and Vibration*, Vol. 344, May 2015, pp. 277–296. doi:10.1016/j.jsv.2015.01.025

[30] Mei, C., Abdel-Motagaly, K., and Chen, R., "Review of Nonlinear Panel Flutter at Supersonic and Hypersonic Speeds," *Applied Mechanics Reviews*, Vol. 52, No. 10, 1999, pp. 321–332. doi:10.1115/1.3098919

[31] Xue, D. Y., and Mei, C., "Finite Element Nonlinear Panel Flutter with Arbitrary Temperatures in Supersonic Flow," *AIAA Journal*, Vol. 31, No. 1, 1993, pp. 154–162. doi:10.2514/3.11332

[32] Guo, X., and Mei, C., "Using Aeroelastic Modes for Nonlinear Panel Flutter at Arbitrary Supersonic Yawed Angle," *AIAA Journal*, Vol. 41, No. 2, 2003, pp. 272–279. doi:10.2514/2.1940

[33] Lee, C. Y., and Kim, J. H., "Aero-Thermoelastic Stability and Nonlinear Flutter Analysis of Functionally Graded Panels," *Journal of Composite Materials*, Vol. 47, No. 18, 2013, pp. 2257–2264. doi:10.1177/0021998312456892

[34] Ibrahim, H. H., and Tawfik, M., "Limit-Cycle Oscillations of Functionally Graded Material Plates Subject to Aerodynamic and Thermal Loads," *Journal of Vibration and Control*, Vol. 16, No. 14, 2010, pp. 2147–2166. doi:10.1177/1077546309353366

[35] Sohn, K. J., and Kim, J. H., "Nonlinear Thermal Flutter of Functionally Graded Panels Under a Supersonic Flow," *Composite Structures*, Vol. 88, No. 3, 2009, pp. 380–387. doi:10.1016/j.compstruct.2008.04.016

[36] Prakash, T., Singha, M. K., and Ganapathi, M., "A Finite Element Study on the Large Amplitude Flexural Vibration Characteristics of FGM Plates Under Aerodynamic Load," *International Journal of Non-Linear Mechanics*, Vol. 47, No. 5, 2012, pp. 439–447. doi:10.1016/j.ijnonlinmec.2011.08.004

[37] Bein, T., Friedmann, P., Zhong, X., and Nydick, I., "Hypersonic Flutter of a Curved Shallow Panel with Aerodynamic Heating," *34th Structures, Structural Dynamics and Materials Conference*, AIAA Paper 1993-1318, April 1993. doi:10.2514/6.1993-1318

[38] Dowell, E. H., "Nonlinear Oscillations of a Fluttering Plate. II," *AIAA Journal*, Vol. 5, No. 10, 1967, pp. 1856–1862. doi:10.2514/3.4316

[39] Liaw, D. G., "Nonlinear Supersonic Flutter of Laminated Composite Plates Under Thermal Loads," *Computers & Structures*, Vol. 65, No. 5, 1997, pp. 733–740. doi:10.1016/S0045-7949(94)00487-0

[40] Stanford, B. K., and Jutte, C. V., "Comparison of Curvilinear Stiffeners and Tow Steered Composites for Aeroelastic Tailoring of Aircraft Wings," *Computers & Structures*, Vol. 183, April 2017, pp. 48–60. doi:10.1016/j.compstruc.2017.01.010

[41] Brake, M. R., Barone, M. F., and Segalman, D. J., "Nonlinear Model Reduction of von Kármán Plates Under Linearized Compressible Fluid Flow," *AIAA Journal*, Vol. 50, No. 5, 2012, pp. 1047–1059. doi:10.2514/1.J050950

[42] Onawola, O. O., and Sinha, S. C., "A Feedback Linearization Approach for Panel Flutter Suppression with Piezoelectric Actuation," *Journal of Computational and Nonlinear Dynamics*, Vol. 6, No. 3, 2011, Paper 031006. doi:10.1115/1.4002391

[43] Dowell, E. H., "Flutter of a Buckled Plate as an Example of Chaotic Motion of a Deterministic Autonomous System," *Journal of Sound and Vibration*, Vol. 85, No. 3, 1982, pp. 333–344. doi:10.1016/0022-460X(82)90259-0

[44] Kouchakzadeh, M. A., Rasekh, M., and Haddadpour, H., "Panel Flutter Analysis of General Laminated Composite Plates," *Composite Structures*, Vol. 92, No. 12, 2010, pp. 2906–2915. doi:10.1016/j.compstruct.2010.05.001

[45] Navazi, H. M., and Haddadpour, H., "Nonlinear Aero-Thermoelastic Analysis of Homogeneous and Functionally Graded Plates in Supersonic Airflow Using Coupled Models," *Composite Structures*, Vol. 93, No. 10, 2011, pp. 2554–2565. doi:10.1016/j.compstruct.2011.04.018

[46] Mei, G., Zhang, J., and Wang, Z., "Numerical Analysis of Panel Flutter on Inertial Manifolds with Delay," *Journal of Computational and Nonlinear Dynamics*, Vol. 8, No. 2, 2013, Paper 021009. doi:10.1115/1.4006948

[47] Brake, M. R., and Segalman, D. J., "Nonlinear Model Reduction of von Kármán Plates Under Quasi-Steady Fluid Flow," *AIAA Journal*, Vol. 48, No. 10, 2010, pp. 2339–2347. doi:10.2514/1.J050357

[48] Xie, D., Xu, M., Dai, H., and Dowell, E. H., "Proper Orthogonal Decomposition Method for Analysis of Nonlinear Panel Flutter with Thermal Effects in Supersonic Flow," *Journal of Sound and Vibration*, Vol. 337, Feb. 2015, pp. 263–283. doi:10.1016/j.jsv.2014.10.038

[49] Xie, D., and Xu, M., "A Simple Proper Orthogonal Decomposition Method for von Karman Plate Undergoing Supersonic Flow," *Computer Modeling in Engineering and Sciences*, Vol. 93, No. 5, 2013, pp. 377–409. doi:10.3970/cmes.2013.093.377

[50] Beran, P. S., Lucia, D. J., and Pettit, C. L., "Reduced-Order Modelling of Limit-Cycle Oscillation for Aeroelastic Systems," *Journal of Fluids and Structures*, Vol. 19, No. 5, 2004, pp. 575–590. doi:10.1016/j.jfluidstructs.2004.04.002

[51] Xie, D., Xu, M., and Dowell, E. H., "Proper Orthogonal Decomposition Reduced-Order Model for Nonlinear Aeroelastic Oscillations," *AIAA Journal*, Vol. 52, No. 2, 2014, pp. 229–241. doi:10.2514/1.J051989

[52] Akhavan, H., and Ribeiro, P., "Natural Modes of Vibration of Variable Stiffness Composite Laminates with Curvilinear Fibers," *Composite Structures*, Vol. 93, No. 11, 2011, pp. 3040–3047. doi:10.1016/j.compstruct.2011.04.027

[53] Akhavan, H., Ribeiro, P., and De Moura, M. F. S. F., "Large Deflection and Stresses in Variable Stiffness Composite Laminates with Curvilinear Fibres," *International Journal of Mechanical Sciences*, Vol. 73, Aug. 2013, pp. 14–26. doi:10.1016/j.ijmecsci.2013.03.013

[54] Akhavan, H., Ribeiro, P., and De Moura, M. F. S. F., "Damage Onset on Tow-Placed Variable Stiffness Composite Laminates," *Composite Structures*, Vol. 113, July 2014, pp. 419–428. doi:10.1016/j.compstruct.2014.03.038

[55] Ribeiro, P., "Non-Linear Free Periodic Vibrations of Variable Stiffness Composite Laminated Plates," *Nonlinear Dynamics*, Vol. 70, No. 2, 2012, pp. 1535–1548. doi:10.1007/s11071-012-0554-4

[56] Ribeiro, P., "Non-Linear Modes of Vibration of Thin Cylindrical Shells in Composite Laminates with Curvilinear Fibres," *Composite Structures*, Vol. 122, April 2015, pp. 184–197. doi:10.1016/j.compstruct.2014.11.019

[57] Ribeiro, P., and Stoykov, S., "Forced Periodic Vibrations of Cylindrical Shells in Laminated Composites with Curvilinear Fibres," *Composite Structures*, Vol. 131, Nov. 2015, pp. 462–478. doi:10.1016/j.compstruct.2015.05.050

[58] Akhavan, H., and Ribeiro, P., "Geometrically Non-Linear Periodic Forced Vibrations of Imperfect Laminates with Curved Fibres by the Shooting Method," *Composites Part B: Engineering*, Vol. 109, No. 15, 2017, pp. 286–296. doi:10.1016/j.compositesb.2016.10.059

[59] Akhavan, H., and Ribeiro, P., "Free Geometrically Nonlinear Oscillations of Perfect and Imperfect Laminates with Curved Fibres by the Shooting Method," *Nonlinear Dynamics*, Vol. 81, Nos. 1–2, 2015, pp. 949–965. doi:10.1007/s11071-015-2043-z

[60] Akhavan, H., and Ribeiro, P., "Non-Linear Forced Periodic Oscillations of Laminates with Curved Fibres by the Shooting Method," *International Journal of Non-Linear Mechanics*, Vol. 76, Nov. 2015, pp. 176–189. doi:10.1016/j.ijnonlinmec.2015.06.004

[61] Akhavan, H., and Ribeiro, P., "Aeroelasticity of Composite Plates with Curvilinear Fibres in Supersonic Flow," *Composite Structures*, Vol. 194, No. 15, 2018, pp. 335–344. doi:10.1016/j.compstruct.2018.03.101

[62] Stanford, B. K., Jutte, C. V., and Wu, K. C., "Aeroelastic Benefits of Tow Steering for Composite Plates," *Composite Structures*, Vol. 118, Dec. 2014, pp. 416–422. doi:10.1016/j.compstruct.2014.08.007

[63] Haddadpour, H., and Zamani, Z., "Curvilinear Fiber Optimization Tools for Aeroelastic Design of Composite Wings," *Journal of Fluids and Structures*, Vol. 33, Aug. 2012, pp. 180–190. doi:10.1016/j.jfluidstructs.2012.05.008

[64] Guimarães, T. A. M., Castro, S. G. P., Rade, D. A., and Cesnik, C. E. S., "Panel Flutter Analysis and Optimization of Composite Tow Steered Plates," *58th AIAA/ASCE/AHS/ASC Structures, Structural Dynamics, and Materials Conference*, AIAA Paper 2017-1118, Jan. 2017. doi:10.2514/6.2017-1118

[65] Tatting, B. F., Gürdal, Z., and Jegley, D., "Design and Manufacture of Elastically Tailored Tow Placed Plates," NASA CR-2002-211919, 2002.

[66] Vlasov, B. F., "On the Equations of Bending of Plates," *Dokla Ak Nauk Azerbeijanskoi-SSR*, Vol. 3, 1957, pp. 955–979.

[67] Reddy, J. N., *Mechanics of Laminated Composite Plates and Shells: Theory and Analysis*, CRC Press, Boca Raton, FL, 2004, Chap. 11. doi:10.1201/b12409

[68] Han, W., Petyt, M., and Hsiao, K. M., "An Investigation into Geometrically Nonlinear Analysis of Rectangular Laminated Plates Using the Hierarchical Finite Element Method," *Finite Elements in Analysis and Design*, Vol. 18, Nos. 1–3, 1994, pp. 273–288. doi:10.1016/0168-874X(94)90107-4

[69] Bardell, N. S., "Free Vibration Analysis of a Flat Plate Using the Hierarchical Finite Element Method," *Journal of Sound and Vibration*, Vol. 151, No. 2, 1991, pp. 263–289. doi:10.1016/0022-460X(91)90855-E

[70] Akhavan, H., "Non-Linear Vibrations of Tow Placed Variable Stiffness Composite Laminates," Ph.D. Thesis, Univ. of Porto, Porto, Portugal, 2015.

[71] Dowell, E. H., Clark, R., Cox, D., Curtiss, H. C., Edwards, J. W., Hall, K. C., Peters, D. A., Scanlan, R., Simiu, E., Sisto, F., et al., *A Modern Course in Aeroelasticity*, Kluwer Academic, Dordrecht, The Netherlands, 2004, Chap. 3.

[72] Amabili, M., *Nonlinear Vibrations and Stability of Shells and Plates*, Cambridge Univ. Press, Cambridge, United Kingdom, 2008, Chap. 15. doi:10.1017/cbo9780511619694

[73] Amabili, M., and Pellicano, F., "Multimode Approach to Nonlinear Supersonic Flutter of Imperfect Circular Cylindrical Shells," *Journal of Applied Mechanics*, Vol. 69, No. 2, 2002, pp. 117–129. doi:10.1115/1.1435366

[74] Meirovitch, L., *Computational Methods in Structural Dynamics*, Springer Science+Business Media, Germany, 1980, Chap. 10.

[75] Ribeiro, P., "On the Influence of Membrane Inertia and Shear Deformation on the Geometrically Non-Linear Vibrations of Open, Cylindrical, Laminated Clamped Shells," *Composites Science and Technology*, Vol. 69, No. 2, 2009, pp. 176–185. doi:10.1016/j.compscitech.2008.09.038

[76] Thomas, W. T., and Dahleh, M. D., *Theory of Vibration with Applications*, Prentice–Hall, New Jersey, 1988, Chap. 11.

[77] Grover, N., Singh, B. N., and Maiti, D. K., "An Inverse Trigonometric Shear Deformation Theory for Supersonic Flutter Characteristics of Multilayered Composite Plates," *Aerospace Science and Technology*, Vol. 52, May 2016, pp. 41–51. doi:10.1016/j.ast.2016.02.017

[78] Srinivas, S., Rao, C. V. J., and Rao, A. K., "An Exact Analysis for Vibration of Simply-Supported Homogeneous and Laminated Thick Rectangular Plates," *Journal of Sound and Vibration*, Vol. 12, No. 2, 1970, pp. 187–199. doi:10.1016/0022-460X(70)90089-1

[79] Reddy, J., and Phan, N., "Stability and Vibration of Isotropic, Orthotropic and Laminated Plates According to a Higher-Order Shear Deformation Theory," *Journal of Sound and Vibration*, Vol. 98, No. 2, 1985, pp. 157–170. doi:10.1016/0022-460X(85)90383-9

[80] Wolf, A., Swift, J. B., Swinney, H. L., and Vastano, J. A., "Determining Lyapunov Exponents from a Time Series," *Physica D: Nonlinear Phenomena*, Vol. 16, No. 3, 1985, pp. 285–317. doi:10.1016/0167-2789(85)90011-9

[81] Rodrigues, J., Ribeiro, P., and Akhavan, H., "Experimental and Finite Element Modal Analysis of Variable Stiffness Composite Laminated Plates," *Proceedings of the 11th International Conference on Vibration Problems*, APMTAC, Portugal, 2013, pp. 978–989.

[82] Ellen, C. H., "Influence of Structural Damping on Panel Flutter," *AIAA Journal*, Vol. 6, No. 11, 1968, pp. 2169–2174. doi:10.2514/3.4951

[83] Kounadis, A. N., "On the Paradox of the Destabilizing Effect of Damping in Non-Conservative Systems," *International Journal of Non-Linear Mechanics*, Vol. 27, No. 4, 1992, pp. 597–609. doi:10.1016/0020-7462(92)90065-F

[84] Oyibo, G. A., "Unified Panel Flutter Theory with Viscous Damping Effects," *AIAA Journal*, Vol. 21, No. 5, 1983, pp. 767–773. doi:10.2514/3.8145

[85] Pigolotti, L., Mannini, C., and Bartoli, G., "Destabilizing Effect of Damping on the Post-Critical Flutter Oscillations of Flat Plates," *Meccanica*, Vol. 52, No. 13, 2017, pp. 3149–3164. doi:10.1007/s11012-016-0604-y

[86] Pigolotti, L., Mannini, C., and Bartoli, G., "Destabilizing Damping Effect on Flat-Plate Vibrations due to Flow-Induced Flutter," *Procedia Engineering, X International Conference on Structural Dynamics*, Vol. 199, EURODYN 2017, 2017, pp. 790–795. doi:10.1016/j.proeng.2017.09.076

[87] Tommasini, M., Kirillov, O. N., Misseroni, D., and Bigoni, D., "The Destabilizing Effect of External Damping: Singular Flutter Boundary for the Pflüger Column with Vanishing External Dissipation," *Journal of the Mechanics and Physics of Solids*, Vol. 91, June 2016, pp. 204–215. doi:10.1016/j.jmps.2016.03.011

[88] Hahn, H. T., and Tsai, S. W., *Introduction to Composite Materials*, Vol. 1, CRC Press, Boca Raton, FL, 1980, Chap. 7.

C. Bisagni
Associate Editor